Semiconductor Physics, Quantum Electronics & Optoelectronics, 2009. V. 12, N 4. P. 406-411.

PACS 42.79.Bh, 78.66.Db, 84.60.Jt

Thin silicon solar cells with SiO_x/SiN_x Bragg mirror rear surface reflector

I.I. Ivanov[1], T.V. Nychyporuk[2], V.A. Skryshevsky[1], M. Lemiti[2]
[1]*Taras Shevchenko Kyiv National University, Faculty of Radiophysics, build. 5, 2, Academician Glushkov prospect, 03022 Kyiv, Ukraine*
E-mail: ivancko@gmail.com
[2]*Institut des Nanotechnologies de Lyon, UMR CNRS 5270, Université de Lyon, INSA Lyon, Bât. Blaise Pascal, 7 avenue Jean Capelle, 69621 Villeurbanne Cedex, France*

Abstract. Bragg reflectors consisting of sequence of dielectric layers with a quarter wavelengths optical thickness are promising to create solar cells of third generation. SiO_x/SiN_x Bragg mirror (BM) at the backside of textured multicrystalline silicon solar cells was fabricated by PECVD method. BM with 9 bi-layers was optimized for the maximum reflectivity within the wavelength range $\Delta\lambda$ = 820...1110 nm. The maximum measured reflectivity is approximately 82 %. Measured reflectivity values were compared with the simulated ones by using the transfer matrix. Effect of parameters for pyramids of several types on the total reflectivity of BM deposited on textured silicon surface was simulated. Enhancement of light absorption and external quantum efficiency in the longwave part of the spectrum (λ > 940 nm) was observed, and it was explained as increase of the photon absorption length. The influence of BM on passivation of SC rear surface was explored. The cell back contact was formed by Al diffusion through BM to the μc-Si wafer and promoted by a pulsed laser. For SC with BM, the efficiency 13.75 % is obtained comparatively with efficiency 13.58 % for SC without BM.

Keywords silicon solar cell, Bragg mirror, numerical simulation.

Manuscript received 11.06.09; accepted for publication 10.09.09; published online 30.10.09.

1. Introduction

Nowadays, the 1st generation of Si solar cells (SC) based on bulk Si technology dominates the photovoltaic market [1]. However, the important limitation of this matured technology is the cost per Watt. In order to reduce the costs of fabrication of Si based SC one of the possible ways is to decrease the volume of primary material involved into this fabrication. Another approach is to increase the photovoltaic conversion efficiency. Indeed, for a single junction Si SC the efficiency limit is only 29 % mainly because of two power losses mechanisms. The first one concerns the absorption by Si SC the high energy photons generating the electron-hole pairs with energy greater than the band gap of Si. The excess of the energy is then dissipated mainly by heat losses. Whereas the second one is inability of SC to absorb the photons with energies less than the band gap of Si. The latter mechanism of losses is not negligible and in the case of standard sun illumination achieves 23.5 % of the total incident power of the sunlight [2]. This effect is even more crucial for thin SC. One of the ways to diminish these losses is to increase the optical path for weakly absorbed photons within the SC [3]. Bragg mirrors (BM) as rear surface reflectors could provide the conditions for multi-passing of IR photons within the SC. BM is a structure of an alternating sequence of layers with different reflection indexes [4]. Each layer has the optical thickness $\lambda_0/4$, where λ_0 – wavelength of BM maximum reflection coefficient. Reflected light components from interfaces between the two layer interfaces interfere, which results in reflection amplification. Schematic representation of paths for infrared light with the intensity I inside SC with and without BM rear reflector is shown in Fig. 1. The reflected light intensity I_R^* for the interface Si/BM and reflected light intensity I_R for the interface Si/air obeys inequality $I_R^* > I_R$ inside the Bragg peak (BP) bandwidth. The transmitted light intensity I_T^* for SC with BM is much less than the transmitted light intensity I_T for SC without BM. These relationships are valid inside the Bragg peak region. After reflection, the low energy photons are returned towards SC bulk.

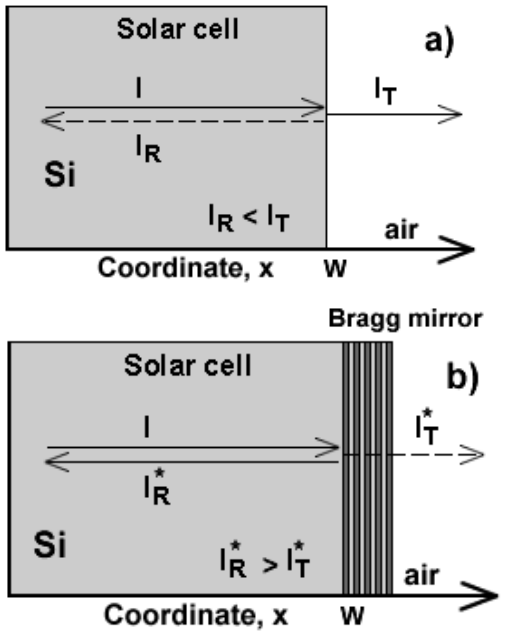

Fig. 1. Schematic representation of paths for infrared light with the intensity *I* inside SC (a) without and (b) with BM, *W* is the SC thickness.

It should be noted that the rear surface passivation is a crucial step for SC fabrication. Hence, the BM realized on the rear surface must satisfy two conditions: assure the reflection of low energy photons and provide good passivation. For this reason, the usual metallic layers evaporated on the back surface of SC cannot be used. On the one hand, the reflection coefficient of metals in the IR spectral region is high enough. For example, for Al it can reach 95 % at 1150 nm. On the other point of view, during the firing process the metals can easily diffuse into the silicon and thus forming a rather considerable number of recombination centers.

Various methods of BM fabrication of the rear surface of silicon SC have already been developed. Duerinck *et al.* have recently reported on fabrication of reorganized porous silicon Bragg reflectors for thin-film silicon SC [5]. Indeed, refractive index of porous silicon can be tuned within the wide range going from 2.7 to 1.3 making it a good candidate for BM fabrication. The authors showed that the stacks of porous silicon layers have been successfully applied to maximize internal reflection at the interface between a silicon substrate and epitaxially grown layer. An optical-path-length enhancement factor of seven was calculated in the wavelength range of 900-1200 nm. The gain of 12 % in short-circuits current and efficiency was thus shown in thin-film epitaxial SC.

Another interesting approach was recently explored. Conducting BM were fabricated on the base of TiO_2 nanostructures [6]. Periodic modulation of the refractive index was achieved by controlling the degree of porosity for each alternate layer through the particle size distribution of the precursor suspensions. Photoelectrochemical measurements show that the BM are conductive and can be a good candidate for rear surface reflector of SC.

However, all these methods cannot be implemented directly for industrial SC fabrication and need crucial changes in the existing photovoltaic technological process. In this work, we report on the SiO_x/SiN_x Bragg rear reflector fabrication for industrial type thin SC. The optical and photoelectrical characteristics of realized SC are discussed in details.

2. Numerical simulation

BM is a structure which consists of an alternating sequence of layers made of two different optical materials with refractive indexes n_H and n_L, the optical thickness of the layers for normal incidence corresponds to $\lambda_0/4$. Other important characteristics of a BM are the reflection coefficient R_{max} at λ_0, the reflection bandwidth λ_{BP} at $0.99R_{max}$, left and right border spectral positions λ_L, λ_R at $0.99R_{max}$.

Evolutions of λ_L and λ_R versus n_H/n_L ratio are presented in Fig. 2 for three different Bragg wavelengths λ_0 (quantity of bi-layers = 10). As can be seen from the figure, the response bandwidth of the BM is wider for layers having a higher refractive index contrast. Left and right spectral borders shift to the short and longwave spectral regions, respectively.

Fig. 3a presents the reflection coefficient of the mirror at the Bragg wavelength versus n_H/n_L ratio for different numbers of layer pairs. The increase in layer pairs results in a higher refection coefficient R_{max} at the Bragg wavelength for a lower ratio value n_H/n_L, but the value of the refection coefficient $R_{max}(\lambda_0) = 99$ % can be obtained for the bi-layer number $N_{bi} = 4$ when $n_H/n_L > 1.8$ (Fig. 3).

The bi-layer number increase from $N_{bi} = 4$ up to 14 leads to BM width increasing (Fig. 3b). For ratio $n_H/n_L = 2$, BM width increases by 31 % when the bi-layer number changes from $N_{bi} = 4$ up to 6. The following bi-layer number increase to $N_{bi} = 14$ does not result in a considerable growth of the BM width λ_{BP}.

The software PC1D [7, 8] was used for simulation of SC parameters. To do that for SC with BM, the following parameters were used: Si wafer thickness was 200 μm, emitter thickness was 500 nm, emitter doping was $N_d = 3 \cdot 10^{20}$ cm^{-3}, base doping was $N_a = 10^{16}$ cm^{-3}, both side texturing with the pyramid base angle 54.74º and pyramid height 5 μm.

The external quantum efficiency (EQE) and *I-V* dependence at various internal front and rear reflection coefficients (R_1, R_2) of sunrays inside the textured Si wafer was calculated (Fig. 4). As can be seen from Fig. 4, using the BM as a backside reflector leads to EQE curve shift to the longwave spectral region at $\lambda > 955$ nm.

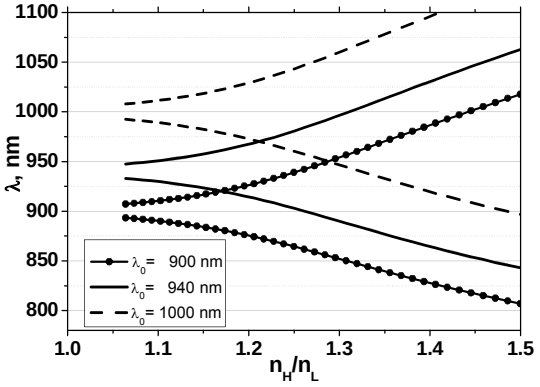

Fig. 2. Response bandwidth of the BM versus n_H/n_L ratio for three different Bragg wavelengths.

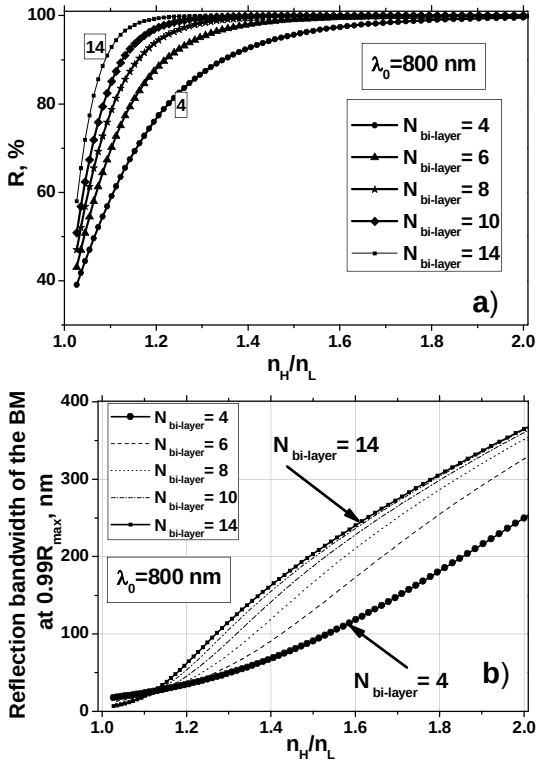

Fig. 3. Dependence of $R_{max}(\lambda_0)$ reflection coefficient (a) and Bragg peak width at $0.99R_{max}$ (digits show the quantity of bi-layers) (b) on n_H/n_L ratio for different bi-layer number.

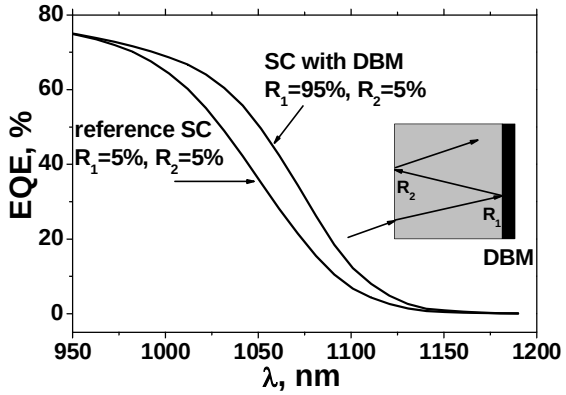

Fig. 4. EQE versus the wavelength for various front and rear internal reflection coefficients (R_1, R_2).

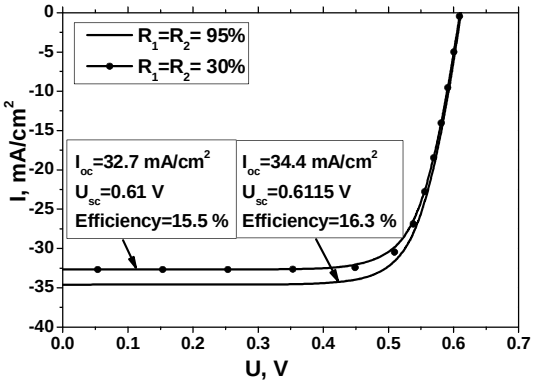

Fig. 5. *I-V* dependence for different values of internal reflection coefficients inside Si wafer.

The simulation results show that the light beam path increase caused by internal multiple beam bouncing inside the wafer leads to the short-current increase (I_{sc}). I_{sc} and SC efficiency increases by 5 % when internal reflection coefficients grow from 20 up to 95 % (Fig. 5).

3. Multicomponent Bragg mirror spectral response simulation

Multicrystalline silicon wafers used for SC production consist of Si grains with various crystal-lattice orientations (CLO) ⟨i⟩ and areas S_i. One of the SC production steps is wafer etching in KOH-base solution for both-side surface texturing in the shape of pyramids. Geometry of etched pyramids is determined by CLO, however, the certain surface grains are badly etched and pyramids do not form. The light beam path inside Si wafer depends on both front and rear SC surface pyramids type and incoming light angle into Si wafer. The reflection coefficient of every grain in Si wafer with BM depends on pyramid parameters because the BM reflection coefficient depends on the light incidence angle. The spectral response of multicrystalline silicon wafer with rear side BM is equal to the sum of BM spectral responses of grain components:

$$R_{m\mathrm{Si}} = \sum_{i=0}^{N} R_i \cdot \sum_{j=1}^{M} S_j^i \,, \tag{1a}$$

$$S_i = \sum_{j=1}^{M} S_j^i \,,\ S = \sum_{i=1}^{N} S_i \,, \tag{1b}$$

where R_i is the reflection coefficient of an elementary Si grain with ⟨i⟩ CLO, S is the total Si wafer area, S_i is the grain area with ⟨i⟩ CLO. The total reflection response of multicrystalline silicon wafer is determined by weighted summation of separate grain reflection coefficients R_i. Weighted coefficients are determined by a cluster with area S_i and reflection coefficients R_i.

Fig. 6 shows the light paths inside the both-side textured wafer ⟨100⟩ with pyramid base angle 54.74º of light beam incidence. The angles on the BM rear side are

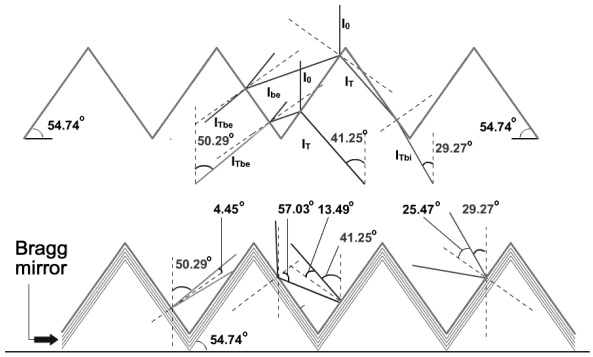

Fig. 6. The light paths inside Si both-side textured wafer ⟨100⟩ at normal beam incidence on SC front.

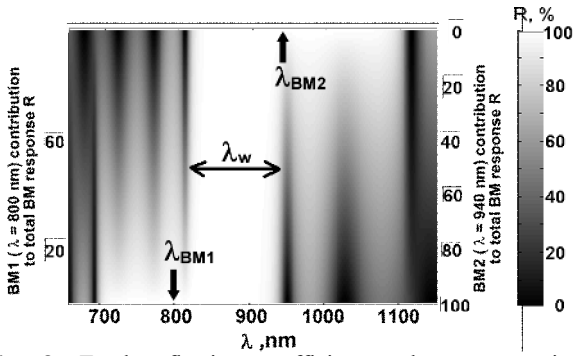

Fig. 8. Total reflection coefficient and separate mirror contributions to total response of two-component BM versus the wavelength (λ_{BM1} = 800 nm and λ_{BM2} = 940 nm, number of bi-layers is 10).

4.45º, 13.49º, 25.45º. The values of internal angles depend on the number of beam reflections from the front side. The total BM spectral response dependence on the incidence angle is shown in Fig. 7. The increase in this angle causes BM position shift to the shortwave spectral region and BM width growth from λ_w^0 up to λ_w^*. The central region on the spectral dependence with a high reflection coefficient (λ_w) remains nonshifted, when the angle of incidence increases from 0º up to 90º.

Fig. 8 shows the simulated spectral dependence of reflection from BM that consists of two grains (BM position at λ_{BM1} = 800 nm and λ_{BM2} = 940 nm). Fig. 8 depicts the reflection coefficient is high at the λ_w region, if the spectral responses of Bragg peaks are overlapped in this region. The resulting spectral response of many-component BM is determined by the position and amplitude of non-main side peaks for BM component. The spectral response of many-component BM is more complicated comparatively with that of the two-component BM.

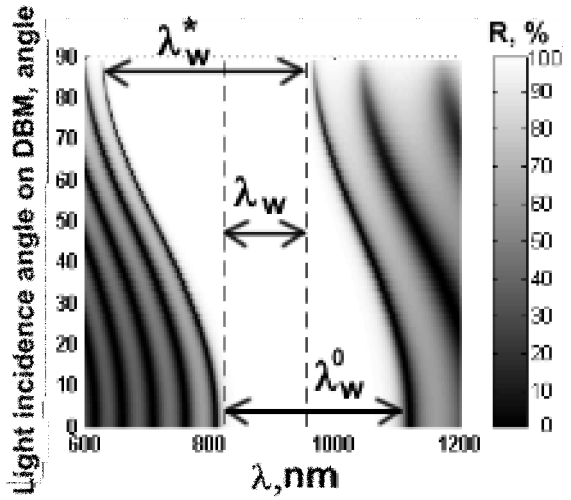

Fig. 7. BM reflection coefficient dependence on the wavelength and incident angle (λ_0 = 940 nm, bi-layer number N_{bi} = 9).

4. Effect of SiO_x /SiN_x Bragg mirror on solar cell parameters

A square *p*-type multicrystalline silicon wafer was used as a base for SC with dielectric Bragg mirror (DBM) manufacturing (N_a = 10^{16} cm^{-3}, wafer size is 125×125 mm, wafer thickness is 200 μm). The emitter thickness and doping were 500 nm and N_d = $3\cdot10^{20}$ cm^{-3}, respectively. The wafer was both-side textured by KOH etching (texturing depth is 5 μm). *p-n* junction was formed after texturing. Back surface field p^+ region was doped up to N_a = $5\cdot10^{18}$ cm^{-3}. Antireflection SiN_x coating was deposited on the front SC surface to decrease front surface reflection. Antireflection coating parameters were chosen to obtain the minimum reflectivity at λ = 600 nm. DBM was formed on rear side of Si wafer by using successive deposition of SiO_x (n_L = 1.46, L_L = 161 nm) and SiN_x (n_H = 2.2, L_H = 107 nm) layers with PECVD method. DBD scheme is depicted in Fig. 9. The total DBM thickness was 2.4 μm. To improve Al diffusion through DBM to Si wafer, DBM was perforated with laser beam (λ_{laser} = 470 nm, P = 1200 mW). The distance between holes was 1.5 mm, hole diameters were 80 μm. Fig. 10 shows SEM image of SC with DBM. DBM layers with different reflection indexes are represented with different intensity bars at the SEM image.

Reflection and transmission coefficients of tested SC with DBM were measured using the integration sphere. The absolute values of reflection and transmission were obtained with calibrated reflection standards.

Spectral dependences of the reflection coefficient of five BMs that were measured from rear SC side are shown in Fig. 11. The reflection coefficients at BM maxima are varied within the range from 63 up to 82 %. Some differences between the experimental curves (SC without DBM No.1 - 2 and SC with DBM No.1 - 5) and the simulated one can be caused by dispersion of reflection indexes in DBM layers, because Si wafers were located at different heights inside the chemical reactor.

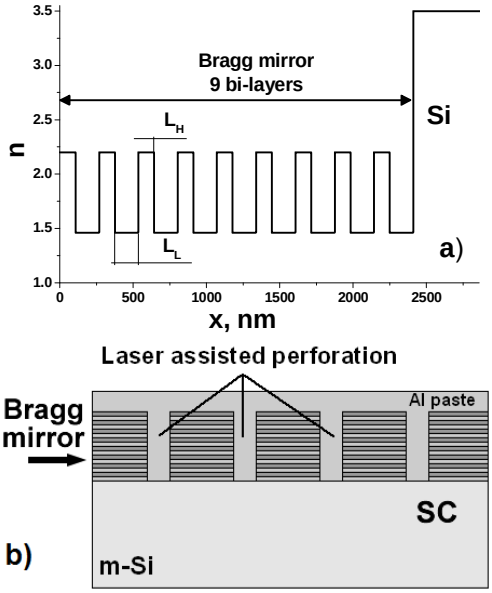

Fig. 9. a) Scheme of SC with DBM on the base of SiN_x/SiO_x; b) scheme of SC rear side with laser assisted perforation through BM.

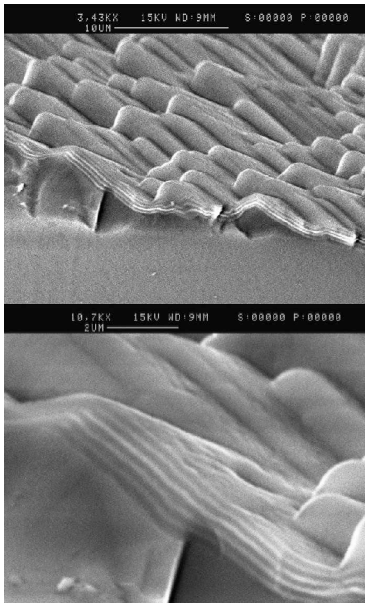

Fig. 10. SEM image of DBM at textured SC rear surface (9 bi-layers).

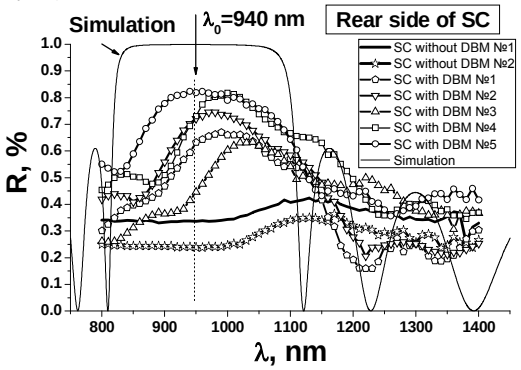

Fig. 11. Simulated and measured reflection dependences of SC with DBM.

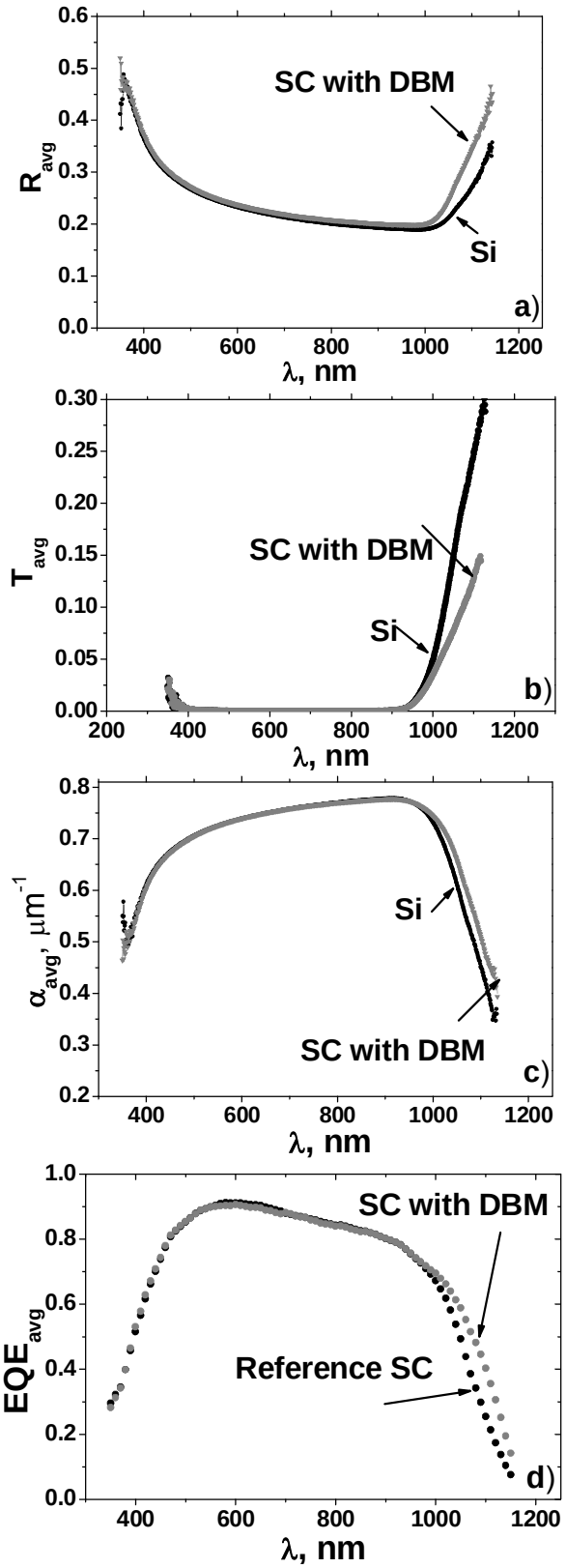

Fig. 12. Comparison of SC with and without DBM: a) spectral dependence of the reflection coefficient; b) spectral dependence of the transmission coefficient; c) spectral dependence of the absorption coefficient; d) spectral dependence of the external quantum efficiency.

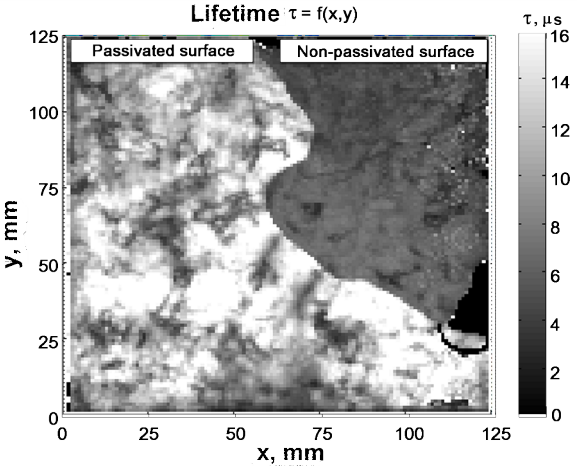

Fig. 13. Lifetime dependence on the surface of SC for passivated and non-passivated parts.

Fig. 12 shows the averaged spectral dependences of the front surface reflection coefficient (Fig. 12a), transmission coefficient (12b), absorption coefficient (12c), EQE for SC with DBM comparatively with those of the sample without DBM. Results of five SC with DBM were used for averaging. The presence of DBM results in increase of the reflection coefficient for DBM, absorption coefficient in SC and EQE within the longwave range. Curves for SC with DBM and without DBM do not differ for the spectral range $\lambda < 1000$ nm.

To verify the passivation effect of DBM presence on the lifetime of minority charge carriers, SC with DBM were annealed for 15 s at 720 ºC in oxygen atmosphere. Fig. 13 shows the mapping of the electron lifetime τ for SC with DBM. For the same wafer, one part was passivated and another was not. The electron lifetime increases after passivation. The presence of DBM does not cause the τ decrease for SC with DBM. The maximal life time of electrons increases from 5.7 up to 11 μs, while the average electron lifetime increases from 5.53 up to 11.14 μs.

Using the SunUoc method [9], the serial resistance value $R_s = 2$ Ohm and pseudo fill factor PFF = 74.7 % (fill factor without R_s effect) were determined. Results of *I-V* dependence analysis are summarized in Table.

Table. Cell parameters.

	I_{sc}, mA/cm^2	U_{oc}, V	FF, %	Efficiency, %
Solar cell with DBM	33	0.587	71	13.75
Solar cell without DBM	32.3	0.584	72	13.58

5. Conclusions

Using the BM allows to improve the absorption in the longwave spectral range due to the photon path increase inside Si wafer. EQE improvement is observed within the spectral range from 940 to 1200 nm. The standard PECVD method can be used to produce BM as a set of SiO_x/SiN_x layers with an optimized BM position and width. The total reflection coefficient of both-side textured SC with DBM depends on geometry of pyramids and their type as well as ratio between different types of pyramids. DBM as a dielectric stack displays also the good passivation properties – the maximum lifetime of minority charge carriers increases from 5.7 up to 11 μs. For SC with DBM, the efficiency was 13.75 % as compared with that 13.58 % for SC without DBM.

References

1. M.A. Green, *Third Generation Photovoltaics: Advanced Solar Energy Conversion.* Springer, Berlin, 2003.
2. M.A. Green, *Solar Cells: Operating Principles, Technology, and System Applications.* Prentice-Hall, New-York, 1982.
3. S.P. Tobin, S.M. Vernon, M.M. Sanfacon, A. Mastrovito, Enhanced light absorption in GaAs solar cells with internal Bragg reflectors // *Photovoltaic specialists conference* **22**(1), p. 147-152 (1991).
4. M. Bass, *Handbook of Optic: Devices, Measurements and Properties.* McGraw-Hill, New-York, 2003.
5. F. Duerinck, I. Kuzma-Filipek, V. Nieuwenhuysen, G. Beaucarne, J. Poortmans, Reorganized porous silicon Bragg reflectors for thin-film silicon solar cells // *Electron Device Lett.* **27**(10), p. 837-839 (2006).
6. M.E. Calvo, S. Colodrero, T.C. Rojas, J.A. Anta, M. Ocaña, H. Míguez, Photoconducting Bragg mirrors based on TiO_2 nanoparticle multilayers // *Advanced Functional Materials* **18**, p. 2708-2715 (2008).
7. D. Rover, P. Basore, A. Smith, PC-1D version 2: enhanced numerical solar cell modeling // *Photovoltaic specialists conference* **20**(1), p. 389-396 (1988).
8. P. Basore, Numerical modeling of textured silicon solar cells using PC-1D // *Electron Devices* **37**(2), p. 337-343 (1990).
9. S. Bowden, A. Rohatgi, Rapid and accurate determination of series resistance and fill factor losses in industrial silicon solar cells // *Proc. of the 17th Europ. PV Solar Energy Conf.*, Munich, 2001.